
ON THE FLY DETECTION OF ROOT CAUSES FROM OBSERVED DATA WITH APPLICATION TO IT SYSTEMS

A PREPRINT

 **Lei Zan**
EasyVista

 **Charles K. Assaad**
EasyVista

 **Emilie Devijver**
Univ. Grenoble Alpes, CNRS,
Grenoble INP, LIG

 **Eric Gaussier**
Univ. Grenoble Alpes, CNRS,
Grenoble INP, LIG

ABSTRACT

This paper introduces a new structural causal model tailored for representing threshold-based IT systems and presents a new algorithm designed to rapidly detect root causes of anomalies in such systems. When root causes are not causally related, the method is proven to be correct; while an extension is proposed based on the intervention of an agent to relax this assumption. Our algorithm and its agent-based extension leverage causal discovery from offline data and engage in subgraph traversal when encountering new anomalies in online data. Our extensive experiments demonstrate the superior performance of our methods, even when applied to data generated from alternative structural causal models or real IT monitoring data.

1 Introduction

IT monitoring systems are described by metrics, as CPU usage, memory usage, or network traffic, and represented by continuous observational time series. In threshold-based IT monitoring systems, predefined thresholds are used to determine when an anomaly or an alert should be triggered [Ligus, 2013], where the thresholds are set manually or through algorithms leveraging offline (i.e., historical) data [Dani et al., 2015]. In IT systems with multiple interconnected subsystems, several metrics may go into an anomalous state during an incident. In this context, root cause analysis consists on identifying actionable root causes of the anomalies that can be used to resolve the incident.

Causal graphs can be used to infer root causes, but obtaining the causal graph from experts can be impractical. Causal discovery methods [Spirtes et al., 2000, Assaad et al., 2022a] have been used to infer causal relations. However, traditional approaches rely on untestable assumptions, require substantial amounts of data, and have been proven to be unsatisfactory for real-world IT monitoring [Aït-Bachir et al., 2023]. This limitation is particularly true when continuous causal relations do not exist in the system, and instead, they emerge in an event-driven manner.

Understanding causal relations between binary thresholded time series can provide more insight than focusing solely on raw time series, offering a clearer identification and analysis of causal relationships. In this paper, we focus on a framework that involves transforming raw time series into binary time series using thresholds. This initial step is followed by the discovery of a causal graph based on the offline binary time series, representing causal relationships between various threshold crossings. As a result, when new anomalies occur in the present, we promptly deduce their root causes directly from both the graph and the time of their appearance using a graph traversal technique.

The remainder of this paper is organized as follows: Section 2 discusses related work. Section 3 introduces a new structural causal model tailored for representing threshold-based IT systems, and Section 4 presents a new algorithm designed to detect root causes of anomalies in such systems. In Section 5, the method is compared to different methods on simulated and real datasets. Finally, Section 6 concludes the paper.

2 State of the Art

Considerable research efforts have recently focused on automated root cause analysis. Some methods utilize causal discovery to uncover causal graphs from anomalous data. For instance, CloudRanger [Wang et al., 2018] employs the

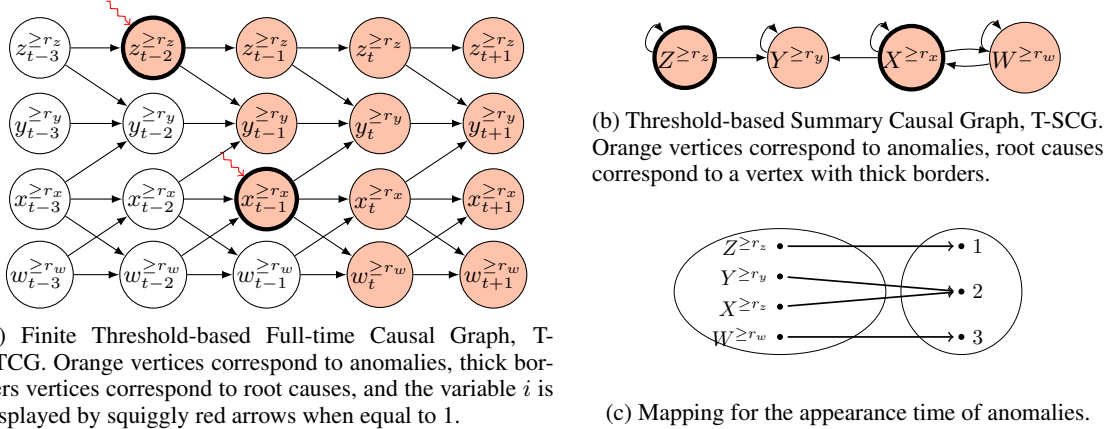


Figure 1: Example. Illustration of (a) a T-FTCG, (b) a T-SCG and (c) the mapping for the appearance time of anomalies on a system with four variables.

PC-algorithm [Spirtes et al., 2000] to discover causal graphs among anomalous time series, then identifies root causes using a random walk strategy based on transition matrices calculated from time series correlations. However, the PC algorithm was not originally designed for time series data, and correlations may not fully capture authentic causal effects. MicroCause Meng et al. [2020] addresses these concerns by utilizing the PCMCI algorithm [Runge et al., 2019] for discovering the causal graph and partial correlations instead of correlations.

Other approaches focus on detecting root causes given the true causal graph of the normal regime. For example, EasyRCA Assaad et al. [2023] identifies some root causes directly from the graph and detects the rest by comparing direct effects in normal and anomalous regimes. CIRCA [Li et al., 2022] employs a service through a graph structure and conducts a regression hypothesis test on anomalous data to identify deviations. However, these methods require a graph as input, which may not always be available. In this paper, we consider a version of EasyRCA and CIRCA where we learn the graph from normal offline data using PCMCI, denoted as EasyRCA* Assaad et al. [2023] and CIRCA*, respectively.

In event-driven systems, event-based causal relations may be more useful. For instance, Van Houdt et al. [2021] introduced a method for identifying root causes within event logs [Rudnitckaia, 2016]. This approach leverages a test hypothesis that considers root causes as variables with the highest conditional dependence with anomalies. However, this method may not be theoretically sound, as shown in an example in the Appendix. Similarly, RCD [Ikram et al., 2022] focuses on discretizing data and identifying root causes through the PC algorithm. However, similarly to CloudRanger and MicroCause, it needs to run the causal discovery algorithm each time an anomaly arises.

From a broader perspective, Wang et al. [2023a] has proposed to model complex systems with interdependent network structures, and detect root causes using hierarchical graph neural networks. Wang et al. [2023b] has used some human feedback in a reinforcement learning fashion to reduce the number of queries. Some methods have also been proposed for inferring root causes of anomalies for non-temporal data, including Budhathoki et al. [2021, 2022]. Those studies are beyond the scope of this paper.

3 Threshold-based causal graphs and root causes

In this section, we present key concepts and assumptions. We employ lowercase letters to represent observed variables, uppercase letters for denoting either name-values or time series, blackboard bold letters for indicating sets (specifically, \mathbb{N} corresponds to the set of integers), and Greek letters to represent constants. A graph is symbolized as \mathcal{G} , with the parents and descendants of a vertex X in \mathcal{G} denoted as $\text{Pa}_{\mathcal{G}}(X)$ and $\text{Desc}_{\mathcal{G}}(X)$, respectively. The indicator function of the event A is expressed as $\mathbb{1}_A$.

In IT systems, the data associated to diverse components of the system is commonly gathered in the form of time series.

Definition 1 (Time series). *For $t \in \mathbb{N}$, consider the random variable $x_t \in [0, 1]$. The sequence $\mathcal{X} = \{x_t; t \in \mathbb{N}\}$ is called a discrete time series. Let \mathbb{V} be the set of name-values of d different discrete time series in a system, $\mathbb{T} = \{\mathcal{X} = \{x_t; t \in \mathbb{N}\}; X \in \mathbb{V}\}$ is called a d -dimensional discrete time series.*

In practical scenarios, time series within IT systems are never observed across an infinite set of time points. This limitation arises due to the operational constraints inherent in IT systems, including specific timeframes, resource constraints, data storage limitations, and operational considerations. Furthermore, the acquisition of time series data is often contingent on the system's monitoring capabilities, which may be characterized by finite recording capacities or designated periods for data collection.

Subsequently, we assume that the random variables in a time series are continuous unless explicitly stated otherwise. However, in many cases, it may be necessary to convert these continuous variables into binary ones through their thresholding. In numerous IT systems, establishing a clear causal connection between two time series, denoted as \mathcal{X} and \mathcal{Y} , is not evident at every time step. Instead, an anomaly in \mathcal{X} can result in an anomaly in \mathcal{Y} : when a specific time point x_t in \mathcal{X} exceeds a predefined threshold, it may trigger a corresponding time point y_t in \mathcal{Y} to breach its own threshold. For instance, consider the monitored time series of network traffic and firewall alerts. Changes in network traffic may not necessarily impact firewall alerts at each time point. However, when network traffic surpasses a threshold, it could signify a security threat, prompting an increase in firewall alerts to signal potential intrusion attempts. In such scenarios, relying solely on raw time series becomes a challenging task. Hereafter, we provide the definition of binary thresholding for time series.

Definition 2 (Binary thresholding of time series). *Consider a discrete time series $\mathcal{X} = \{x_t; t \in \mathbb{N}\}$ and a fixed threshold $r_x \in [0, 1]$. A binary thresholding of \mathcal{X} is the sequence $\mathcal{X}^{\geq r_x} = \{\mathbb{1}_{x_t \geq r_x}; t \in \mathbb{N}\}$.*

Each binary random variable in the sequence $\mathcal{X}^{\geq r_x}$ is represented as $x_t^{\geq r_x}$, where $t \in \mathbb{N}$. Additionally, the binary thresholding of a d -dimensional time series \mathbb{T} is the vector comprising the binary thresholdings of the respective time series.

Simultaneously, investigating causal connections among binary thresholded time series provides a more effective and intuitive perspective for understanding causal relations in these systems. The subsequent definition introduces the concept of a causal graph over binary thresholded d -dimensional time series.

Definition 3 (Threshold-based full-time causal graph, T-FTCG). *Let \mathbb{T} be a d -dimensional discrete time series in a system, \mathbb{V} the set of their name-values and \mathbb{R}^d the set of d potential thresholds, each corresponding to a name-value in \mathbb{V} . A threshold-based full time causal graph $\mathcal{G}_{ft} = (\mathbb{T}^r, \mathbb{E}_{\mathbb{T}}^r)$ is an infinite directed acyclic graph where the set of vertices \mathbb{T}^r corresponds to the set of variables in the binary thresholding of \mathbb{T} and where the set of edges $\mathbb{E}_{\mathbb{T}}^r$ is defined as follows: for two time series $\mathcal{X}, \mathcal{Y} \in \mathbb{T}$, $\forall x_{t-\gamma} \in \mathcal{X}$, and $\forall y_t \in \mathcal{Y}$, $x_{t-\gamma}^{\geq r_x} \rightarrow y_t^{\geq r_y}$ in $\mathbb{E}_{\mathbb{T}}^r$ if and only if $x_{t-\gamma}^{\geq r_x}$ causes $y_t^{\geq r_y}$ at time t with a time lag of $\gamma > 0$.*

An example of a T-FTCG is depicted in Figure 1a (without instantaneous causal relation). To establish a connection between the T-FTCG and the observational data, we adopt the following standard assumptions.

Assumption 1 (Causal Markov condition). *Let $\mathcal{G}_{ft} = (\mathbb{T}^r, \mathbb{E}_{\mathbb{T}}^r)$ be a T-FTCG. For each thresholded time series $\mathcal{X}^{\geq r_x} \in \mathbb{T}^r$, each vertex $x_t^{\geq r_x}$ is independent of its non descendants in \mathcal{G}_{ft} given its parents $Pa_{\mathcal{G}_{ft}}(x_t^{\geq r_x})$.*

Assumption 2 (Adjacency faithfulness). *Let $\mathcal{G}_{ft} = (\mathbb{T}^r, \mathbb{E}_{\mathbb{T}}^r)$ be a T-FTCG. Each two adjacent vertices are statistically dependent given any set of vertices.*

Note that a T-FTCG only shows what are the causes of an effect. We show how an effect is influenced by its causes in the following definition of a threshold-based dynamic structural causal model.

Definition 4 (Threshold-based dynamic structural causal model, T-DSCM). *A threshold-based dynamic structural causal model associated with a T-FTCG $\mathcal{G}_{ft} = (\mathbb{T}^r, \mathbb{E}_{\mathbb{T}}^r)$ is a quadruple $\mathcal{M} = \langle (\mathbb{U}_t, \mathbb{I}_t), \mathbb{T}^r, f, (P(u_t), P(i_t)) \rangle$ where*

1. \mathbb{U}_t and \mathbb{I}_t are two sets of d -dimensional binary background time series (also called exogenous time series), such that each binary variables $u_t^y \in U_t^y$ and $i_t^y \in I_t^y$, where $U_t^y \in \mathbb{U}_t$, $I_t^y \in \mathbb{I}_t$, $Y \in \mathbb{V}$ and $t \in \mathbb{N}$, are determined by factors outside the model;
2. \mathbb{T}^r is a d -dimensional binary observed time series (also called endogenous time series), such that each binary variable $y_t^{\geq r_y} \in \mathcal{Y}^{\geq r_y}$, where $\mathcal{Y}^{\geq r_y} \in \mathbb{T}^r$ and $t \in \mathbb{N}$, is determined by variables in the model;
3. for $\mathcal{Y}^{\geq r_y} \in \mathbb{T}^r$ and $t \in \mathbb{N}$, the structural mapping function is given by, for $u_t^y \in U_t^y$ and $i_t^y \in I_t^y$, where $U_t^y \in \mathbb{U}_t$, $I_t^y \in \mathbb{I}_t$,

$$\begin{aligned} y_t^{\geq r_y} &:= f(Pa_{\mathcal{G}_{ft}}(y_t^{\geq r_y}), u_t^y, i_t^y) \\ &:= \left(\left(\bigvee_{x_{t-\gamma}^{\geq r_x} \in Pa_{\mathcal{G}_{ft}}(y_t^{\geq r_y})} x_{t-\gamma}^{\geq r_x} \right) \wedge u_t^y \right) \vee i_t^y; \end{aligned}$$

4. for all $u_t^y \in U_t^y \in \mathbb{U}_t$, $P(u_t^y) = \text{Bernoulli}(\epsilon_t^y)$ with $\epsilon_t^y \in (0, 1]$ and for all $i_t^y \in I_t^y \in \mathbb{I}_t$, $P(i_t^y) = \text{Bernoulli}(\beta_t^y)$ with $\beta_t^y \in (0, 1)$.

Note that the background variable u_t^y represents the non-immunity of $y_t^{\geq r_y}$ (i.e., if $u_t^y = 0$ then $y_t^{\geq r_y}$ is not affected by its parents in the T-FTSCG) and u_t^y is sampled from a Bernoulli distribution with parameter ϵ_t^y , representing the probability of non-immunity. For example, when $\epsilon_t^y = 1$, if any value in the parents of $y_t^{\geq r_y}$ is equal to 1 then $y_t^{\geq r_y}$ will deterministically be equal to 1. We avoid the case when $\epsilon_t^y = 0$ because, in this scenario, the causal relation between $y_t^{\geq r_y}$ and its parents would be absent. Similarly, the background variable i_t^y represents a hidden cause that deterministically affects $y_t^{\geq r_y}$ (i.e., $i_t^y = 1$ then $y_t^{\geq r_y} = 1$ independently of its parents in the T-FTSCG) and i_t^y is sampled from a Bernoulli distribution with parameter β_t^y . We avoid the cases when $\beta_t^y = 0$ (respectively $\beta_t^y = 1$) to avoid $y_t^{\geq r_y}$ being always equal to 1 (respectively 0).

The T-DSCM relies on the following standard assumption, implying the absence of *unobserved* confounding biases in the system.

Assumption 3. Let $\mathcal{M} = \langle (\mathbb{U}_t, \mathbb{I}_t), \mathbb{T}^r, f, (P(u_t), P(i_t)) \rangle$ be a T-DSCM. We assume that all variables u_t^y and i_t^y of the background time series \mathbb{U}_t and \mathbb{I}_t in \mathcal{M} are jointly independent.

Now we can define anomalies and root causes when considering a T-DSCM associated to a T-FTCG.

Definition 5 (Anomaly). Let $\mathcal{M} = \langle (\mathbb{U}_t, \mathbb{I}_t), \mathbb{T}^r, f, (P(u_t), P(i_t)) \rangle$ be a T-DSCM associated to a T-FTCG $\mathcal{G}_{ft} = (\mathbb{T}^r, \mathbb{E}_{\mathbb{T}}^r)$ and a sample satisfying \mathcal{M} . The random variable $x_t^{\geq r_x} \in \mathbb{T}^r$ is said to be anomalous if $x_t^{\geq r_x} = 1$.

Definition 6 (Root cause). Let $\mathcal{M} = \langle (\mathbb{U}_t, \mathbb{I}_t), \mathbb{T}^r, f, (P(u_t), P(i_t)) \rangle$ be a T-DSCM associated to a T-FTCG \mathcal{G}_{ft} and a sample satisfying \mathcal{M} . The value $x_t^{\geq r_x} \in \mathbb{T}^r$ is said to be a root cause if $i_t^x = 1$.

For illustration, when the vertex $x_t^{\geq r_x}$ exhibits an anomaly, it will be shaded in orange, and if it serves as a root cause, we will enhance its border thickness compared to other vertices, as depicted in Figure 1.

Note that, from the definition of a T-DSCM, each variable has a non-negative probability of being a root cause ($\epsilon_t^y \in (0, 1)$), all root causes are anomalies (if $i_t^y = 1$ then $y_t^{\geq r_y} = 1$), and each anomaly is either propagated from a root cause through a chain of anomalies or is itself a root cause (if $y_t^{\geq r_y} = 1$ either $i_t^y = 1$ or $\exists x_{t-\gamma}^{\geq r_x} \in \text{Pa}_{\mathcal{G}_{ft}}(y_t^{\geq r_y})$ such that $x_{t-\gamma}^{\geq r_x} = 1$ and $u_t^y = 1$).

Our primary objective is to identify the root causes directly from time series data using predefined thresholds. To achieve this goal, we plan to employ causal discovery algorithms, making use of historical data to infer a causal graph. However, the challenge arises from the fact that the full-time causal graph is inherently infinite. Under the following assumption, the T-FTCG becomes finite (sometimes called a window causal graph Assaad et al. [2022a]):

Assumption 4. Let \mathcal{G}_{ft} be a T-FTCG. All the causal relationships remain constant in direction throughout time in \mathcal{G}_{ft} .

This assumption suggests that the edges in the T-FTCG are consistently the same across time (consistency throughout time). We denote γ_{\max} the minimum temporal lag required to construct the smallest finite T-FTCG for which Assumption 4 is satisfied. This parameter also corresponds to the maximal temporal lag between a cause and its effect that exists in the system.

In many applications, comprehending and validating the finite T-FTCG can be challenging for system experts. Additionally, due to its potential largeness, represented by γ_{\max} , errors may occur in finite sample size estimation or when determining the exact lag between a cause and its effect. Consequently, it is more convenient to rely on an abstraction of the T-FTCG.

Definition 7 (Threshold-based Summary Causal Graph, T-SCG). Let \mathbb{V} be the set of name-value of d different time series in a system, \mathbb{R}^d a set of d thresholds, each corresponding to a name-value in \mathbb{V} , and $\mathcal{G}_{ft} = (\mathbb{T}^r, \mathbb{E}_{\mathbb{T}}^r)$ the corresponding T-FTCG. The threshold-based summary causal graph $\mathcal{G} = (\mathbb{V}^r, \mathbb{E}^r)$ associated to \mathcal{G}_{ft} is given by $\mathbb{V}^r := \{X^{\geq r_x} \mid \forall X \in \mathbb{V} \text{ and } r_x \in \mathbb{R}^d\}$ and \mathbb{E}^r such that $X^{\geq r_x} \rightarrow Y^{\geq r_y}$ is in \mathbb{E}^r if and only if there exists $\gamma \in \{1, \dots, \gamma_{\max}\}$ such that $x_{t-\gamma}^{\geq r_x} \rightarrow y_t^{\geq r_y}$ in $\mathbb{E}_{\mathbb{T}}^r$.

For illustration, we present in Figure 1b the T-SCG associated to the T-FTCG introduced in Figure 1a. While the T-FTCG is presumed to be acyclic, its corresponding T-SCG can be cyclic.

Finally, we introduce the appearance time of anomalies.

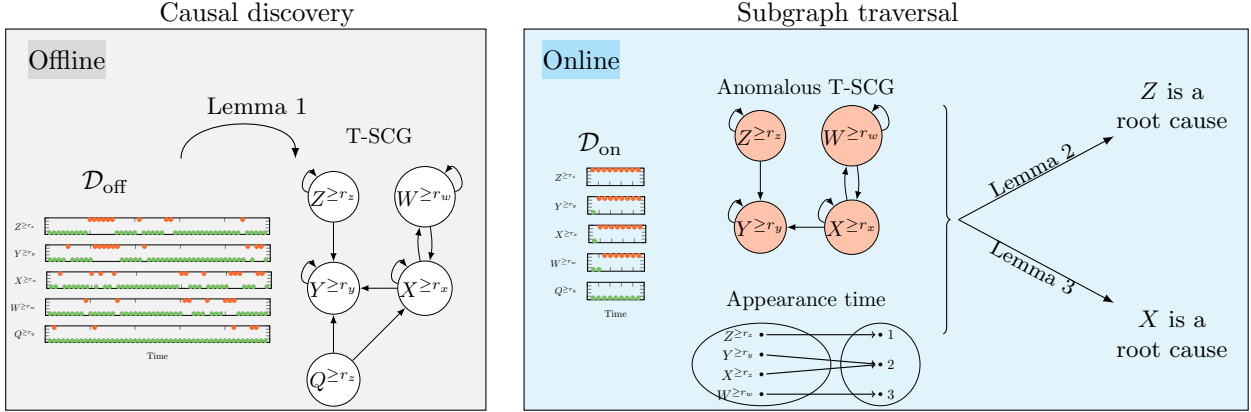


Figure 2: Overview of T-RCA. First step, on the offline dataset: a T-SCG is learned from \mathcal{D}_{off} . Second step, the anomalous T-SCG is deduced from the online dataset, as well as the appearance time. Last step, detection of the root causes using Lemmas 2 and 3.

Definition 8 (Appearance time of anomalies). *Given a T-SCG $\mathcal{G} = (\mathbb{V}^r, \mathbb{E}^r)$ and observations of the time series, the appearance time of anomalies is the mapping*

$$\begin{aligned} \tau : \mathbb{V}^r &\rightarrow \mathbb{N} \\ X^{\geq r_x} &\mapsto \operatorname{argmin}_t \{x_t^{\geq r_x} = 1\}. \end{aligned}$$

This notion of appearance time of anomalies is illustrated in Figure 1c.

4 Threshold-based root cause analysis

In an IT monitoring system, our focus is typically on identifying the root causes of existing anomalies, i.e., those presently occurring in the system. Therefore, we establish a distinction between historical data, referred to as offline data denoted as \mathcal{D}_{off} , and current data, referred to as online data denoted as \mathcal{D}_{on} . Anomalies and root causes will be sought within the online data \mathcal{D}_{on} .

We propose a method called T-RCA (Threshold-based Root Cause Analysis) to detect root causes. This method involves employing causal discovery to first uncover the T-SCG from the offline data \mathcal{D}_{off} . Subsequently, whenever anomalies are detected in the online data \mathcal{D}_{on} , a graph traversal strategy is applied on the inferred T-SCG. An overview of our method is provided in Figure 2.

In Section 4.1, we outline the causal discovery step. Section 4.2 details the graph traversal step and provides the result that, under an additional assumption, our method precisely identifies the set of root causes. Finally, Section 4.3 introduces an extension of T-RCA applicable when the mentioned additional assumption is violated.

4.1 Causal discovery of T-SCG

Pearl [1988] asserts that, in the absence of instantaneous relations, under some assumptions, a directed and acyclic causal graph may be discovered from observational data. We restate precisely this result in the context of T-FTCG.

Lemma 1. *Let \mathcal{M} be a T-DSCM associated to a T-FTCG \mathcal{G}_{ft} . If Assumptions 1, 2, 3, 4 are satisfied then \mathcal{G}_{ft} is identifiable from the distribution induced by \mathcal{M} .*

In practice, any causal discovery algorithm capable of handling binary time series and aligned with our assumptions can be employed. In the experimental section, we specifically utilize the PCMI algorithm [Runge et al., 2019], a temporal adaptation of the PC algorithm [Spirtes et al., 2000], which operates without requiring any additional assumption.

Algorithm 1: T-RCA

Data: Two datasets \mathcal{D}_{off} and \mathcal{D}_{on} of d -dimensional observational time series \mathbb{T} , maximum lag γ_{\max} , set of thresholds for each time series \mathbb{R}^d

Result: Set of root causes $\hat{\mathbb{C}}$

Provide the binary thresholded time series according to thresholds \mathbb{R}^d

Discover the T-SCG $\hat{\mathcal{G}} = (\mathbb{V}^r, \mathbb{E}^r)$ using an event-based causal discovery algorithm on \mathcal{D}_{off} and \mathbb{R}^d // Lemma 1

Deduce the set of anomalous vertices $\mathbb{A} \subseteq \mathbb{V}^r$ from \mathcal{D}_{on} using Definition 5

Deduce the mapping of appearance time of anomalies τ from $\hat{\mathcal{G}}$ and \mathcal{D}_{on} using Definition 8

$\hat{\mathbb{C}} = \emptyset$

```

foreach  $SCC \mathbb{S} \in \hat{\mathcal{G}}_{\mathbb{A}}$  do
  if  $Pa_{\hat{\mathcal{G}}_{\mathbb{A}}}(\mathbb{S}) \subseteq \mathbb{S}$  then
    if  $\text{size}(\mathbb{S}) = 1$  then
       $\hat{\mathbb{C}} = \hat{\mathbb{C}} \cup \mathbb{S}$  // Lemma 2
    else
       $\hat{\mathbb{C}} = \hat{\mathbb{C}} \cup \{X^{\geq r_x}\}$  such that  $X^{\geq r_x} \in \mathbb{S}$  and  $\tau(X^{\geq r_x}) < \tau(Y^{\geq r_y}) \forall Y^{\geq r_y} \in \mathbb{S} \setminus \{X^{\geq r_x}\}$  // Lemma 3
  
```

Once we get the inferred T-FTCG $\hat{\mathcal{G}}_{\text{ft}}$, we can easily deduce the T-SCG $\hat{\mathcal{G}}$ using Definition 7. It is also possible to directly discover the T-SCG (assuming no instantaneous relations) without passing by a T-FTCG as proposed in Assaad et al. [2022b]¹.

4.2 Searching for root causes through subgraph traversal

Let's assume that we observe a T-SCG $\mathcal{G} = (\mathbb{V}^r, \mathbb{E}^r)$ and some online data \mathcal{D}_{on} from which anomalies are observed. The goal is to detect the root causes. We can construct a colored graph, where a vertex is colored if it exhibits an anomaly in the online data \mathcal{D}_{on} . We denote the colored vertices as \mathbb{A} , and $\mathcal{G}_{\mathbb{A}}$ the anomalous subgraph, which contains only colored vertices.

We start by decomposing this graph into strongly connected components, introduced as follows.

Definition 9 (Strongly connected component, (SCC)). *Let $\mathcal{G} = (\mathbb{V}^r, \mathbb{E}^r)$ be a T-SCG. A subset $\mathbb{S} \subseteq \mathbb{V}^r$ is a strongly connected component of \mathcal{G} iff \mathbb{S} is a maximal set of vertices where every vertex is reachable via a directed path in \mathcal{G} from every other vertex in \mathbb{S} .*

For instance, in Figure 1b, there are three SCCs: $\{Z^{\geq r_z}\}$, $\{Y^{\geq r_y}\}$, and $\{X^{\geq r_y}, W^{\geq r_w}\}$.

For each SCC of size 1, we use the following lemma to test if the vertex in the SCC is a root cause.

Lemma 2. *Let $\mathcal{G}_{\mathbb{A}}$ be an anomalous subgraph of a T-SCG $\mathcal{G} = (\mathbb{V}^r, \mathbb{E}^r)$ in \mathcal{D}_{on} . If an anomalous vertex in $\mathcal{G}_{\mathbb{A}}$ does not have any anomalous parent in $\mathcal{G}_{\mathbb{A}}$ then it is a root cause.*

This lemma offers a direct method to identify certain root causes. For instance, in Figure 2, it detects $Z^{\geq r_z}$ as a root cause.

Furthermore, using the notion of appearance time of anomalies, for each SCC of size greater than 1, we use the following lemma to test if one of the vertices in the SCC is a root cause.

Lemma 3. *Let $\mathcal{G}_{\mathbb{A}}$ be an anomalous subgraph of a T-SCG $\mathcal{G} = (\mathbb{V}^r, \mathbb{E}^r)$ in \mathcal{D}_{on} , τ be the appearance time of anomalies, and \mathbb{S} an SCC in $\mathcal{G}_{\mathbb{A}}$ of $\text{size}(\mathbb{S}) > 1$ such that $Pa_{\mathcal{G}_{\mathbb{A}}}(\mathbb{S}) \subseteq \mathbb{S}$. The vertex*

$$\underset{X^{\geq r_x} \in \mathbb{S}}{\operatorname{argmin}} \{\tau(X^{\geq r_x})\}$$

is a root cause.

In our example, using this lemma, we can deduce that $X^{\geq r_x}$ is a root cause since $\tau(X^{\geq r_x}) < \tau(Y^{\geq r_y})$ and $\tau(X^{\geq r_x}) < \tau(W^{\geq r_w})$.

¹The idea proposed in Assaad et al. [2022b], consider a richer type of graph called extended summary causal graph. However, in the case where there are no instantaneous relations, the summary causal graph gives the same information as the extended summary causal graph.

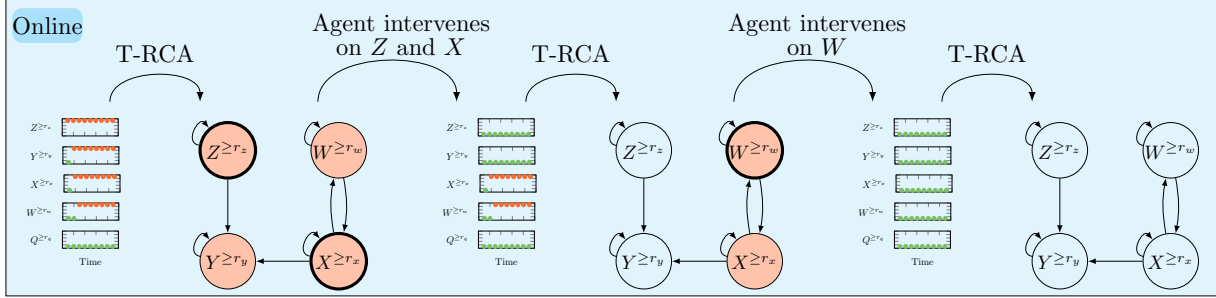


Figure 3: TRCA-agent in practice.

It is noteworthy that the aforementioned lemmas generally do not guarantee the detection of all root causes. Specifically, these lemmas are incapable of detecting a root cause that is influenced by another root cause, i.e., $i_t^y = 1$ and simultaneously $\exists x_{t-\gamma}^{>r_x} \in \text{Pa}_{\mathcal{G}_{\text{ft}}}(y_t^{>r_y})$ such that $x_{t-\gamma}^{>r_x} \wedge u_t^y = 1$. This means that in Figure 1a, if $z_{t-2}^{>r_z}$ is a root cause then $y_{t-1}^{>r_y}$ cannot be a root cause. We argue that these undetectable root causes are rare in practice, therefore we introduce the following assumption to mitigate their impact².

Assumption 5. Let $\mathcal{G} = (\mathbb{V}^r, \mathbb{E}^r)$ be a T-SCG. We assume that if $X^{>r_x}$ is a root cause in \mathcal{D}_{on} , i.e., $\exists t \in \mathcal{D}_{\text{on}}$ such that $i_t^x = 1$, then there exists no $Z^{>r_z} \in \text{Ang}(X^{>r_x})$, such that

- $Z^{>r_z}$ is a root cause in \mathcal{D}_{on} , i.e. $\exists t' \in \mathcal{D}_{\text{on}}$ such that $i_{t'}^z = 1$; and
- for all $Y^{>r_y} \in \text{Desc}_{\mathcal{G}}(Z^{>r_z}) \cap \text{Ang}(X^{>r_x}) \setminus \{X^{>r_x}, Z^{>r_z}\}$, $Y^{>r_y}$ is anomalous in \mathcal{D}_{on} , i.e., $\exists t'' \in \mathcal{D}_{\text{on}}$ such that $y_{t''}^{>r_y} = 1$.

In general, a T-FTCG provides a more detailed representation of the system compared to a T-SCG. However, given the absence of instantaneous relations in the system, the appearance time of anomalies and Assumption 5, the T-FTCG does not confer any advantage in detecting the root cause compared to the T-SCG.

The pseudo-code of T-RCA is presented in Algorithm 1 and the following theorem establishes its correctness under assumption 5.

Theorem 1. Under Assumptions 1, 2, 3, 4, 5, T-RCA detects exactly the set of true root causes: if \mathbb{C} is the set of true root causes and $\hat{\mathbb{C}}$ is the set of root causes inferred by T-RCA, $\mathbb{C} = \hat{\mathbb{C}}$.

4.3 Agent-based extension

When Assumption 5 is violated, T-RCA struggles to distinguish the root causes among the set of anomalies. To address this, we propose an agent-based extension of T-RCA, denoted as T-RCA-agent.

T-RCA-agent initiates by running T-RCA to identify the first batch of root causes associated with anomalies. Subsequently, an agent is activated to rectify the incidents attributed to these root causes. If some anomalies persist, T-RCA-agent reruns T-RCA on the remaining anomalous time series. This iterative process continues until no anomalies remain.

For example, in Figure 3, we observe a T-SCG containing four anomalous vertices X, Y, Z, W with Z, X, W being root causes. Notably, in this illustration, Assumption 5 is violated since W is a root cause that is affected by another root cause. In this scenario, the T-RCA agent begins by employing T-RCA to identify Z and X as root causes. Subsequently, the agent addresses the incident associated with Z and X , resolving anomalies within Z, X , and Y . Following this, T-RCA-agent reruns T-RCA to pinpoint W as a root cause, and the agent rectifies the incident on W . Consequently, all vertices return to normal, leading to the termination of T-RCA-agent.

Unlike T-RCA, T-RCA-agent is guaranteed to detect the root causes even when Assumption 5 is violated. Additionally, theoretically, we know what is the number of iterations needed for the algorithm to terminate. This is given by the following proposition.

²It might appear that under Assumption 5, the time of anomaly and/or the association (possibly conditional) between anomalies might be sufficient to detect root causes. However, it turns out that this is not true as it is shown in Appendix B via several examples, highlighting the crucial role of the causal discovery step.

Proposition 1. *Let m be the maximum number of root causes on the same directed path in the T-SCG and not satisfying Assumption 5. Under Assumptions 1, 2, 3, 4, T-RCA-agent identifies all root causes after m iterations.*

5 Experiments

In this section, we first describe the experimental setup, then conduct a thorough analysis using simulated data generated from several models to evaluate our method, and finally we present an analysis using a real-world IT monitoring dataset³.

5.1 Experimental setup

T-RCA For causal discovery, we use the PCMCI algorithm [Runge et al., 2019] in which the G-squared test, adapted for binary thresholding of time series, is employed to find conditional independencies.

Baselines We compare our methods with 8 other methods: RCD, CloudRanger Wang et al. [2018], MicroCause Meng et al. [2020], EasyRCA and EasyRCA* Assaad et al. [2023], CIRCA and CIRCA* Li et al. [2022] and AITIA-PM Van Houdt et al. [2021]. Note that for simulated data, results of EasyRCA and CIRCA are excluded as they require a causal graph input, which we assume unavailable. However, these results are provided in Appendices C. For RCD, CIRCA*, and AITIA-PM, we select the top two variables from their output ranking as inferred root causes, considering that each case has two genuine root causes. For T-RCA, EasyRCA*, and MicroCause, we set the maximum lag γ_{\max} to 1, and maintain a fixed significance level of 0.01 across all methods. For EasyRCA*, CloudRanger, and MicroCause, a Fisher-z-test is utilized due to their use of raw (continuous) data as input. Additionally, in the case of CloudRanger and MicroCause, the walk length is set to 1000, and the backward step threshold is fixed to 0.1. Finally, other hyperparameters in CIRCA* and RCD are retained as specified in their packages.

Evaluation To evaluate the accuracy of root cause detection, we use the following F1-score between \mathbb{C} and $\hat{\mathbb{C}}$, the sets of real and inferred root causes respectively:

$$F1\text{-score}(\mathbb{C}, \hat{\mathbb{C}}) = \frac{2 \sum_{c \in \mathbb{C}} \mathbb{1}_{c \in \hat{\mathbb{C}}}}{2 \sum_{c \in \mathbb{C}} \mathbb{1}_{c \in \hat{\mathbb{C}}} + \sum_{\hat{c} \in \hat{\mathbb{C}}} \mathbb{1}_{\hat{c} \notin \mathbb{C}} + \sum_{c \in \mathbb{C}} \mathbb{1}_{c \notin \hat{\mathbb{C}}}}.$$

5.2 Simulated data

We consider three settings, each characterized by distinct data generation processes. In the initial setting, we assess the effectiveness of our method by generating data from a T-DSCM. In the second and third settings, we evaluate the robustness of our method by generating data from a model different to a T-DSCM.

Within each setting, we explore two cases: one where Assumption 5 holds, and another where it is violated. In the latter case, we introduce the T-RCA-agent into the comparison and set the number of iterations equal to the maximum number of genuine root causes in an active path. During simulation, for T-RCA-agent, if it successfully identifies a genuine root cause at the end of the iteration, anomalous variables in \mathcal{D}_{on} are adjusted accordingly. This mimics the implementation of actions taken by system engineers to repair the systems. Across all settings, we consider \mathcal{D}_{off} of length 20,000, while we vary the lengths of \mathcal{D}_{on} in $\{10, 20, 50, 100, 200\}$. Additionally, results up to a length of 2,000 are presented in Appendix C.1.

5.2.1 Threshold-based system

The first data generation process considered is based on the T-DSCM stated in Definition 4. We randomly generate 50 T-SCGs, each composed of 6 vertices, with a maximal degree ranging between 4 and 5, and exactly one root vertex. All lags in the T-FTCG associated with these T-SCGs are set to 1. Subsequently, we generate one dataset for each T-SCG.

Each time series is scaled to $[0, 1]$, with thresholds randomly selected from $U([0.7, 0.9])$. Each time series includes a self-cause, and $\epsilon_t^y < 1$, with a probability of 0.3 that an anomalous parent in the T-SCG will not trigger anomalies in its children. Additional cases are provided in Appendix C.2.

For \mathcal{D}_{off} , interventions are applied to each normal variable with a probability $\beta_t^y = 0.1$, causing the variable to exceed its threshold. We ensure that the duration of being anomalous for one time series does not exceed 5 consecutive time

³ A Python code of our method and of all experiments is provided at <https://github.com/leizan/T-RCA>.

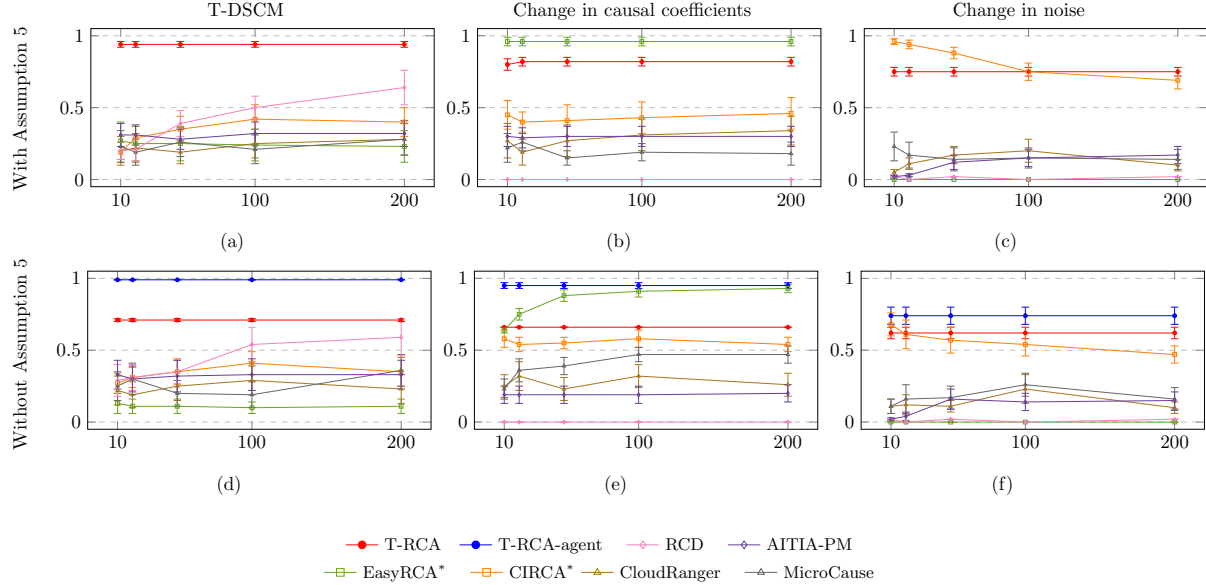


Figure 4: Average F1-score and its variance across 50 simulations are depicted for simulated data. The length of \mathcal{D}_{on} ranges from 10 to 200, generated from a T-DSMC (a and d), a DSCM with root causes experiencing changes in causal coefficients (b and e), and a DSCM with root causes undergoing changes in noise (c and f). Each model is assessed under two settings: one adhering to Assumption 5 (a, b, and c) and another that violates Assumption 5 (d, e, and f).

points. For \mathcal{D}_{on} , if Assumption 5 holds, two vertices on the same active path within the T-SCG are randomly chosen. Otherwise, two vertices on different active paths are randomly chosen.

Results depicting the means and variances of the F1-score for each method are presented in Figure 4(a) and (d), with and without Assumption 5 respectively, where the values of thresholds are presumed to be known. Robustness against misspecification of the thresholds has been tested and is illustrated in Appendix C.3.2. Notably, when Assumption 5 holds, T-RCA consistently outperforms other methods, exhibiting low variance. The performance of T-RCA remains stable since it only requires knowledge of the anomalous variables in \mathcal{D}_{on} . However, in the other case, the performance of T-RCA declines due to the violation of Assumption 5, while T-RCA-agent demonstrates superior performance. All other methods have very low performances. Note that, as the length of \mathcal{D}_{on} increases, the performance of RCD improves.

5.2.2 Non-threshold based system with changes in causal coefficients

To evaluate the robustness of our method, we utilize a dataset introduced by Assaad et al. [2023] comprising 50 different Acyclic Summary Causal Graphs with self-causes. All lags are set to 1. \mathcal{D}_{off} is generated using the DSCM:

$$y_t = \sum_{x_{t-1} \in \text{Pa}_{\mathcal{G}_{ft}}(y_t)} a x_{t-1} + 0.1 \xi_t^y,$$

with $a \sim U([0.1, 1])$, $\xi_t^y \sim N(0, 1)$, y_t denotes the value of the vertex y at time t , $\text{Pa}_{\mathcal{G}_{ft}}(y_t)$ denotes the direct parents of y_t in the FTCG. For \mathcal{D}_{on} , similar to the previous setting, two different strategies are used to randomly select two vertices in each graph for intervention, which are considered as the root causes. The intervention changes the coefficients from all parents of the intervened variable by resampling them from $U([0.1, 1])$. The effect of each intervention propagates through the generating process to all the descendants of the intervened vertex.

Thresholds for each time series are chosen empirically such that each variable in \mathcal{D}_{off} contains 90% of data below the threshold and 10% above it. In this setting, T-RCA and T-RCA-agent utilize thresholds to learn the T-SCG from \mathcal{D}_{off} . The selected root causes and their descendants in the graph are considered as anomalous variables, and this information is utilized by our proposed method, EasyRCA*, CloudRanger, and MicroCause.

Results depicting the means and variances of the F1-score for each method are presented in Figure 4 (b) and (e) for both cases. When Assumption 5 holds, EasyRCA* performs well with low variance, as the data generating process aligns with its settings. The performance of T-RCA follows EasyRCA*, outperforming other methods. In the other

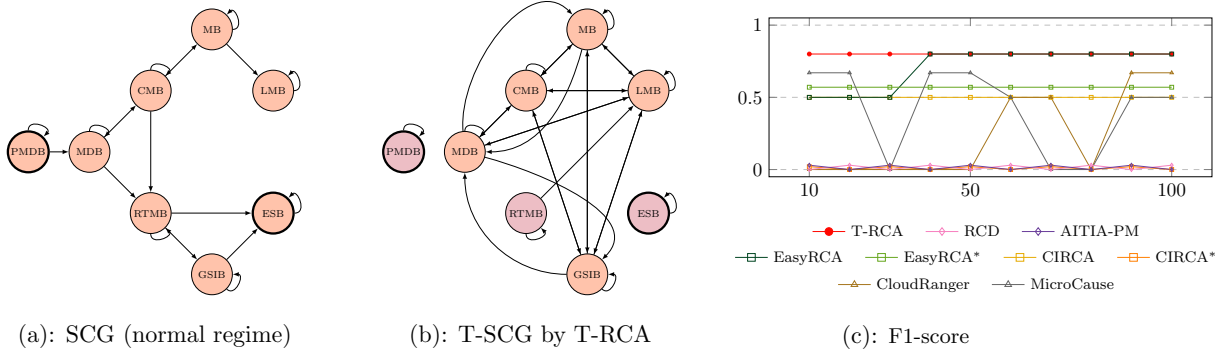


Figure 5: Real IT monitoring data: (a) the SCG provided by the experts, on the normal regime, where root causes correspond to the vertices with thick borders (PMDB and ESB); (b) the T-SCG learned by T-RCA, where inferred root causes correspond to purple vertices (PMDB and ESB); (c) F1-score for the IT monitoring data, varying the lengths of \mathcal{D}_{on} from 10 to 100.

case, T-RCA suffers, while the performance of EasyRCA* increases along with the expansion of the length of \mathcal{D}_{on} . Notably, T-RCA-agent exhibits a comparable performance with EasyRCA*, and even better for a small length of \mathcal{D}_{on} .

5.2.3 Non-threshold based system with changes in noise

Finally, we utilize a dataset simulating a microservice architecture from the DoWhy package⁴. The graph consists of 11 vertices, and a lag of 1 is assumed between each pair of vertices to simulate time series data. Similar to the previous setting, two different strategies are used to randomly select two vertices in the graph for intervention. We generate 50 datasets for each case. Interventions are applied following Scenario 3 in the provided link, which involves shifting the value by a constant. Thresholds for each time series are determined by using the empirical strategy described earlier.

Results depicting the means and variances of the F1-score for each method are presented in Figure 4 (c) and (f) for both cases. When Assumption 5 holds, CIRCA* exhibits good performance with a small length of \mathcal{D}_{on} . However, its performance declines as \mathcal{D}_{on} increases. T-RCA shows reasonable performance and outperforms other methods when \mathcal{D}_{on} exceeds 100. When Assumption 5 is violated, T-RCA-agent consistently outperforms other methods, followed by T-RCA and CIRCA*. Similar to the previous setting, the performance of CIRCA* declines as the length of \mathcal{D}_{on} increases. These methods clearly outperform others in both cases.

5.3 Real IT monitoring data

The dataset, provided by EasyVista and introduced in Assaad et al. [2023], consists of eight time series collected from an IT monitoring system with a one-minute sampling rate, as described in Assaad et al. [2023], Aït-Bachir et al. [2023].

For T-RCA and AITIA-PM methods, which rely on anomalies in historical data for root cause detection, consider all data preceding the onset of anomalies as \mathcal{D}_{off} , comprising more than 40,000 data points. However, for methods needing only normal data as \mathcal{D}_{off} , we use 1,000 data points from the normal part before anomalies. We vary the length of \mathcal{D}_{on} from 10 to 100 with a step of 10. Thresholds for each time series are selected such that each variable in \mathcal{D}_{off} contains 90% of data below the threshold and 10% above it, with robustness tested in Appendix C.3.2. Each time series is anomalous within \mathcal{D}_{on} . For CIRCA, we consider only one ultra-metric, *Saturation*. Due to the inability to simulate system engineer interventions, T-RCA-agent is not part of the comparison.

The true T-SCG associated with this system is unknown, but EasyVista’s system experts have described the summary causal graph in the normal regime (when there are no anomalies), which is provided in Figure 5(a). Thus, for methods needing a graph, such as CIRCA and EasyRCA, the summary causal graph in the normal regime serves as the input graph. PMDB and ESB are expected to be the root causes of the anomalies. The T-SCG learned by T-RCA is given in Figure 5(b). The graph is denser than the SCG stated in Figure 5(a), but they do not encode the same information. Most importantly, the genuine root causes are discovered.

⁴https://www.pywhy.org/dowhy/v0.11.1/example_notebooks/gcm_rca_microservice_architecture.html

The F1-score of each method is presented in Figure 5(c). T-RCA consistently performs well, achieving an F1-score of 0.8, similar to EasyRCA which knows the SCG in the normal regime, when the length of \mathcal{D}_{on} exceeds 30. CIRCA and EasyRCA* exhibit reasonable performance. Meanwhile, the result also exhibits the importance of the correct causal graph for the method CIRCA and EasyRCA. The performance of CloudRanger and MicroCause varies considerably, influenced by random mechanisms in their respective methods.

6 Conclusion

We introduced a new structural causal model designed to represent threshold-based IT systems, and we presented the T-RCA algorithm for detecting root causes of anomalies in such systems. In its simplest form, T-RCA assumes the absence of more than one root cause in an active path aligned with the causal graph derived from the structural causal model. Additionally, we presented an optimized agent-based extension of T-RCA, relaxing this assumption while requiring minimal actions within the system. Our experiments demonstrated that our methods outperform other methods, particularly on data generated from the considered structural causal model, and showcased its effectiveness even on data from alternative structural causal models.

For future work, it would be interesting to consider instantaneous relations. In this case, having richer graphs, which are inherently acyclic, can offer advantages, especially when anomalies form a cycle in the T-SCG. Furthermore, we assumed that all variables of the background time series \mathbb{U}_t and \mathbb{I}_t are jointly independent, but this is a strong assumption in practice, it would be interesting to relax this. Finally, it would be interesting to explore solutions that alleviate Assumption 5 without requiring external actions. We note that on the considered real dataset, it has not been an issue, and this assumption can be reasonable on sparse graphs.

Acknowledgements

This work has been partially supported by MIAI@Grenoble Alpes (ANR-19-P3IA-0003) and by EasyVista. We thank Ali Aït-Bachir, Christophe de Bignicourt and Hosein Mohanna from EasyVista for providing the IT monitoring data and for several discussions about threshold-based IT systems.

References

- C. K. Assaad, E. Devijver, and E. Gaussier. Survey and evaluation of causal discovery methods for time series. *Journal of Artificial Intelligence Research*, 73:767–819, feb 2022a.
- C. K. Assaad, E. Devijver, and E. Gaussier. Discovery of extended summary graphs in time series. In J. Cussens and K. Zhang, editors, *Proceedings of the Thirty-Eighth Conference on Uncertainty in Artificial Intelligence*, volume 180 of *Proceedings of Machine Learning Research*, pages 96–106. PMLR, 01–05 Aug 2022b.
- C. K. Assaad, I. Ez-zejjari, and L. Zan. Root cause identification for collective anomalies in time series given an acyclic summary causal graph with loops. In F. Ruiz, editor, *Proceedings of the Twenty-Sixth Conference on Artificial Intelligence and Statistics*, Proceedings of Machine Learning Research. PMLR, April 2023.
- A. Aït-Bachir, C. K. Assaad, C. de Bignicourt, E. Devijver, S. Ferreira, E. Gaussier, H. Mohanna, and L. Zan. Case studies of causal discovery from it monitoring time series. submitted, 2023.
- K. Budhathoki, D. Janzing, P. Bloebaum, and H. Ng. Why did the distribution change? In A. Banerjee and K. Fukumizu, editors, *Proceedings of The 24th International Conference on Artificial Intelligence and Statistics*, volume 130 of *Proceedings of Machine Learning Research*, pages 1666–1674. PMLR, 13–15 Apr 2021.
- K. Budhathoki, L. Minorics, P. Bloebaum, and D. Janzing. Causal structure-based root cause analysis of outliers. In K. Chaudhuri, S. Jegelka, L. Song, C. Szepesvari, G. Niu, and S. Sabato, editors, *Proceedings of the 39th International Conference on Machine Learning*, volume 162 of *Proceedings of Machine Learning Research*, pages 2357–2369. PMLR, 17–23 Jul 2022.
- M.-C. Dani, F.-X. Jollois, M. Nadif, and C. Freixo. Adaptive threshold for anomaly detection using time series segmentation. In *Neural Information Processing: 22nd International Conference, ICONIP 2015, Istanbul, Turkey, November 9–12, 2015, Proceedings Part III 22*, pages 82–89. Springer, 2015.
- A. Ikram, S. Chakraborty, S. Mitra, S. Saini, S. Bagchi, and M. Kocaoglu. Root cause analysis of failures in microservices through causal discovery. In S. Koyejo, S. Mohamed, A. Agarwal, D. Belgrave, K. Cho, and A. Oh, editors, *Advances in Neural Information Processing Systems*, volume 35, pages 31158–31170. Curran Associates, Inc., 2022.

- M. Li, Z. Li, K. Yin, X. Nie, W. Zhang, K. Sui, and D. Pei. Causal inference-based root cause analysis for online service systems with intervention recognition. In *Proceedings of the 28th ACM SIGKDD Conference on Knowledge Discovery and Data Mining*, KDD '22, page 3230–3240, New York, NY, USA, 2022. Association for Computing Machinery. ISBN 9781450393850. doi: 10.1145/3534678.3539041.
- S. Ligus. *Effective Monitoring and Alerting*. O'Reilly, 2013. ISBN 9781449333522.
- Y. Meng, S. Zhang, Y. Sun, R. Zhang, Z. Hu, Y. Zhang, C. Jia, Z. Wang, and D. Pei. Localizing failure root causes in a microservice through causality inference. In *2020 IEEE/ACM 28th International Symposium on Quality of Service (IWQoS)*, pages 1–10, 2020. doi: 10.1109/IWQoS49365.2020.9213058.
- J. Pearl. *Probabilistic Reasoning in Intelligent Systems: Networks of Plausible Inference*. Morgan Kaufmann, 1988.
- J. Rudnitckaia. Process mining. data science in action. *University of Technology, Faculty of Information Technology*, pages 1–11, 2016.
- J. Runge, P. Nowack, M. Kretschmer, S. Flaxman, and D. Sejdinovic. Detecting and quantifying causal associations in large nonlinear time series datasets. *Science Advances*, 5(11):eaau4996, 2019. doi: 10.1126/sciadv.aau4996.
- P. Spirtes, C. N. Glymour, R. Scheines, and D. Heckerman. *Causation, prediction, and search*. MIT press, 2000.
- G. Van Houdt, B. Depaire, and N. Martin. Root cause analysis in process mining with probabilistic temporal logic. In *International Conference on Process Mining*, pages 73–84. Springer, 2021.
- D. Wang, Z. Chen, J. Ni, L. Tong, Z. Wang, Y. Fu, and H. Chen. Interdependent causal networks for root cause localization. In *Proceedings of the 29th ACM SIGKDD Conference on Knowledge Discovery and Data Mining*, KDD '23, page 5051–5060, New York, NY, USA, 2023a. Association for Computing Machinery.
- L. Wang, C. Zhang, R. Ding, Y. Xu, Q. Chen, W. Zou, Q. Chen, M. Zhang, X. Gao, H. Fan, S. Rajmohan, Q. Lin, and D. Zhang. Root cause analysis for microservice systems via hierarchical reinforcement learning from human feedback. In *Proceedings of the 29th ACM SIGKDD Conference on Knowledge Discovery and Data Mining*, KDD '23, page 5116–5125, New York, NY, USA, 2023b. Association for Computing Machinery.
- P. Wang, J. Xu, M. Ma, W. Lin, D. Pan, Y. Wang, and P. Chen. Cloudranger: Root cause identification for cloud native systems. In *2018 18th IEEE/ACM International Symposium on Cluster, Cloud and Grid Computing*, pages 492–502. IEEE, 2018.

A Proofs

Lemma 1. *Let \mathcal{M} be a T-DSCM associated to a T-FTCG \mathcal{G}_{ft} . If Assumptions 1, 2, 3, 4 are satisfied then \mathcal{G}_{ft} is identifiable from the distribution induced by \mathcal{M} .*

Sketch of proof. We present here a sketch of proof, and refer the interested reader to Pearl [1988] for more details. The identifiability of the causal graph is given by the temporal order of variables, which states that a cause precedes the effect in time. Additionally, according to the causal Markov condition, we can effectively determine the independence between a vertex and its non-descendants given its parents. Consider the historical dataset \mathcal{D}_{off} . We can initialize a graph $\hat{\mathcal{G}}_R$ where, for all vertices $(y_t^{\geq r_y}, x_{t-\gamma}^{\geq r_x}) \in \mathbb{T}^r$, for $\gamma > 0$, $x_{t-\gamma}^{\geq r_x} \rightarrow y_t^{\geq r_y}$. Then, we test conditional independences to remove edges, with the adjacency faithfulness assumption ensuring that the excluded variables are not parents of $y_t^{\geq r_y}$. This process leaves only those variables that persist as parents of $y_t^{\geq r_y}$ in $\hat{\mathcal{G}}_{ft}$. \square

Lemma 2. *Let \mathcal{G}_A be an anomalous subgraph of a T-SCG $\mathcal{G} = (\mathbb{V}^r, \mathbb{E}^r)$ in \mathcal{D}_{on} . If an anomalous vertex in \mathcal{G}_A does not have any anomalous parent in \mathcal{G}_A then it is a root cause.*

Proof. By Definition 4, the anomaly on a vertex $Y^{\geq r_y}$ that does not have any anomalous parent cannot be propagated from other vertices, i.e., $\left(\left(\bigvee_{x_{t-\gamma}^{\geq r_x} \in Pa_{\mathcal{G}_{ft}}(y_t^{\geq r_y})} x_{t-\gamma}^{\geq r_x} \right) \wedge u_t^y \right) = 0$. Thus i_t^y has to be equal to 1 which implies that $Y^{\geq r_y}$ is a root cause. \square

Lemma 3. *Let \mathcal{G}_A be an anomalous subgraph of a T-SCG $\mathcal{G} = (\mathbb{V}^r, \mathbb{E}^r)$ in \mathcal{D}_{on} , τ be the appearance time of anomalies, and \mathbb{S} an SCC in \mathcal{G}_A of $\text{size}(\mathbb{S}) > 1$ such that $Pa_{\mathcal{G}_A}(\mathbb{S}) \subseteq \mathbb{S}$. The vertex*

$$\operatorname{argmin}_{X^{\geq r_x} \in \mathbb{S}} \{\tau(X^{\geq r_x})\}$$

is a root cause.

Proof. Let \mathbb{S} be an SCC in an anomalous subgraph $\mathcal{G}_{\mathbb{A}}$ such that $\text{size}(\mathbb{S}) > 1$ and $\text{Pa}_{\mathcal{G}_{\mathbb{A}}}(\mathbb{S}) \subseteq \mathbb{S}$. By Definition 4, the anomaly on $Y^{\geq r_y}$ satisfying $\underset{X^{\geq r_x} \in \mathbb{S}}{\text{argmin}}\{\tau(X^{\geq r_x})\}$ cannot be propagated from other vertices, i.e., $\left(\left(\bigvee_{x_{t-\gamma}^{\geq r_x} \in \text{Pa}_{\mathcal{G}_{\mathbb{A}}}(y_t^{\geq r_y})} x_{t-\gamma}^{\geq r_x} \right) \wedge u_t^y \right) = 0$. Thus u_t^y has to be equal to 1 which implies that $Y^{\geq r_y}$ is a root cause. \square

Theorem 1. *Under Assumptions 1, 2, 3, 4, 5, T-RCA detects exactly the set of true root causes: if \mathbb{C} is the set of true root causes and $\hat{\mathbb{C}}$ is the set of root causes inferred by T-RCA, $\mathbb{C} = \hat{\mathbb{C}}$.*

Proof. The proof of soundness (an inferred root cause by T-RCA is necessarily a true root cause) of the method is directly given by Lemmas 2 and 3.

What is left to prove is that under Assumption 5, a true root cause is necessarily inferred by T-RCA. Suppose that there exists $C \in \mathbb{C}$ such that C is not detectable by T-RCA. Then,

- C is not a root vertex in the anomalous subgraph of the T-SCG (otherwise it would have been detected by Lemma 2), and
- C does not belong to an SCC \mathbb{S} such that \mathbb{S} is of size greater than 1 and $\text{Pa}_{\mathcal{G}_{\mathbb{A}}}(\mathbb{S}) \subseteq \mathbb{S}$ (otherwise it would have been detected by Lemma 3).

If C is not a root vertex and it belongs to an SCC \mathbb{S} of size 1 then C violates Assumption 5, since in this case, C has necessarily a parent that is anomalous and is either a root cause or is propagated from a root cause that is an ancestor of C . If C is not a root vertex and it belongs to an SCC \mathbb{S} of size greater than 1 and $\text{Pa}_{\mathcal{G}_{\mathbb{A}}}(\mathbb{S}) \not\subseteq \mathbb{S}$ then C also violates Assumption 5, since in this case, at least one member of \mathbb{S} has an anomalous parent that is not in \mathbb{S} and that is either a root cause or is propagated from a root cause that is an ancestor of C ; all other members have an anomalous parent in \mathbb{S} that is propagated from a root cause that is an ancestor of C . \square

Proposition 1. *Let m be the maximum number of root causes on the same directed path in the T-SCG and not satisfying Assumption 5. Under Assumptions 1, 2, 3, 4, T-RCA-agent identifies all root causes after m iterations.*

Proof. Using Theorem 1, only the root cause at the beginning of each directed path is identified. Subsequently, after the intervention of an agent, the number of root causes in each directed path decreases by at least 1 (even though multiple interventions may occur simultaneously, T-RCA selects one randomly), maintaining the maximum number of root causes on a directed path at $m - 1$. Anomalous variables in \mathcal{D}_{on} are updated accordingly, and another root cause may become the root in this directed path. By induction, after employing T-RCA m times, all root causes are detected. \square

B Examples of Insufficiency of correlation and time

It might appear that under Assumption 5, the time of anomaly and/or the association (possibly conditional) between anomalies might be sufficient to detect root causes. We provide two examples showing that this is, in fact, not true, highlighting the crucial role of the causal discovery step.

Example 1 (Insufficiency of time and dependence). *Consider a scenario involving three time series, where the underlying T-SCG among them are depicted in Figure 6 (a). The lag between X and Y is 1, while the lag between X and Z is 2. Assuming $\epsilon_t^y < 1$ and ignoring self-causes, multiple interventions are applied to X at different time steps to induce anomalies.*

When identifying the root cause(s) of $Z^{\geq r_z} = 1$ (denoted as $Z_{=1}^{\geq r_z}$) solely based on temporal information, both $X_{=1}^{\geq r_x}$ and $Y_{=1}^{\geq r_y}$ are included, as they occur before $Z_{=1}^{\geq r_z}$. Similarly, solely relying on dependence also points to both $X_{=1}^{\geq r_x}$ and $Y_{=1}^{\geq r_y}$ as root causes, given their connections to $Z_{=1}^{\geq r_z}$. Even when considering temporal and dependence information together, $Y_{=1}^{\geq r_y}$ remains identified as the root cause.

Example 2 (Insufficiency of time and conditional dependence on a single variable). *Consider another scenario involving four time series, where the underlying T-SCG among them is depicted in Figure 6 (b). The lag between W , X and Z , X is 1, while the lag between W , Y and Z , Y is 2. Assuming $\epsilon_t^y < 1$ (i.e., uncertainty in anomaly propagation) and ignoring self-causes, multiple interventions are applied independently on W and Z at different time steps to induce anomalies. Here, we aim to detect all root causes of $Y^{\geq r_y} = 1$ (denoted as $Y_{=1}^{\geq r_y}$).*



Figure 6: (a) demonstrates a scenario where time and dependence fail to detect all root causes. (b) demonstrates a scenario where time and conditional dependence on a single variable fail to detect all root causes.

Firstly, using temporal order, $W_{=1}^{>r_w}$, $X_{=1}^{>r_x}$ and $Z_{=1}^{>r_z}$ are considered as potential causes of $Y_{=1}^{>r_y}$ because they precede it.

Then, using dependence conditioning on a single variable cannot guarantee the detection of root causes. For example, when conditioning on $W_{=1}^{>r_w}$ (resp. $Z_{=1}^{>r_z}$), $X_{=1}^{>r_x}$ becomes dependent on $Y_{=1}^{>r_y}$, because of $Z_{=1}^{>r_z}$ (resp. $W_{=1}^{>r_w}$). Consequently, $X_{=1}^{>r_x}$ is incorrectly considered a root cause.

Even using a special measure that sums over multiple conditional dependence, we will not be able to guarantee the detection of root causes: as previously, between $X_{=1}^{>r_x}$ and $Y_{=1}^{>r_y}$, even though we do a sum of multiple terms of conditional dependence, but within each term, we only condition on one variable, which will not break the dependence between these two variables.

Furthermore, even if we search for the highest conditional dependence, as done in AITIA-PM [Van Houdt et al., 2021], there is no guarantee to find all root causes. For instance, consider again the T-SCG in Figure 6 (b), but now assume $\epsilon_t^y = 1$. Then, the special measure (used by AITIA-PM) that sums over multiple conditional dependence between $Y_{=1}^{>r_y}$ and $X_{=1}^{>r_x}$ is :

$$\{ \Pr(Y_{=1}^{>r_y} | X_{=1}^{>r_x} \wedge W_{=1}^{>r_w}) - \Pr(Y_{=1}^{>r_y} | X_{=0}^{>r_x} \wedge W_{=1}^{>r_w}) \\ + \Pr(Y_{=1}^{>r_y} | X_{=1}^{>r_x} \wedge Z_{=1}^{>r_z}) - \Pr(Y_{=1}^{>r_y} | X_{=0}^{>r_x} \wedge Z_{=1}^{>r_z}) \} = 2$$

which is higher than the same special measure between $Y_{=1}^{>r_y}$ and $Z_{=1}^{>r_z}$ equal to:

$$\{ \Pr(Y_{=1}^{>r_y} | W_{=1}^{>r_w} \wedge Z_{=1}^{>r_z}) - \Pr(Y_{=1}^{>r_y} | W_{=0}^{>r_w} \wedge Z_{=1}^{>r_z}) \\ + \Pr(Y_{=1}^{>r_y} | W_{=1}^{>r_w} \wedge X_{=1}^{>r_x}) - \Pr(Y_{=1}^{>r_y} | W_{=0}^{>r_w} \wedge X_{=1}^{>r_x}) \} = 0.$$

C Complementary experiments

C.1 Extension of Section 5.2 - varying the length of \mathcal{D}_{on}

In Figure 7, we present the results of the means and variances of the F1-score for each method, considering a larger length of \mathcal{D}_{on} up to 2,000 samples. These results align with the three settings delineated in Section 5.2. In addition, in this analysis, we include the results of EasyRCA and CIRCA, which require a causal graph as input.

Results corresponding to the setting in Section 5.2.1 are presented in Figure 7 (a and d). In this setting, when Assumption 5 holds, EasyRCA exhibits comparable performance with T-RCA, and even performs better when the length of \mathcal{D}_{on} is small. However, its performance declines as the length of \mathcal{D}_{on} increases due to an increased number of tests. When Assumption 5 is violated, the performance of EasyRCA decreases significantly, but it tends to improve as the length of \mathcal{D}_{on} expands, particularly when it exceeds 100 samples. In both cases, the performance of RCD tends to improve with the increasing length of \mathcal{D}_{on} , while CIRCA demonstrates comparable performance with CIRCA*.

Results corresponding to the setting in Section 5.2.2 are presented in Figure 7 (b and e). In this setting, when Assumption 5 holds, EasyRCA outperforms other methods. In the other case, EasyRCA outperforms other methods when the length of \mathcal{D}_{on} exceeds 200, as the setting aligns well with the design of EasyRCA. CIRCA exhibits an intermediate performance in both cases.

Results corresponding to the setting in Section 5.2.3 are presented in Figure 7 (c and f). In the setting, when Assumption 5 holds, EasyRCA shows comparable performance with T-RCA and even outperforms it. In the other case,

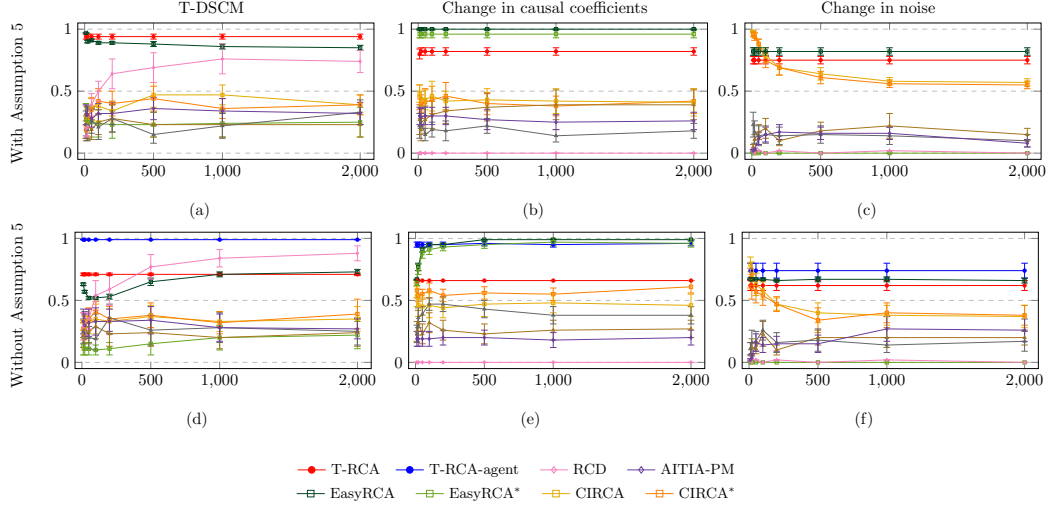


Figure 7: Mean of F1-score averaged over 50 simulations, and associated variance, for the three data generating processes, the lengths of \mathcal{D}_{on} varying from 10 to 2,000.

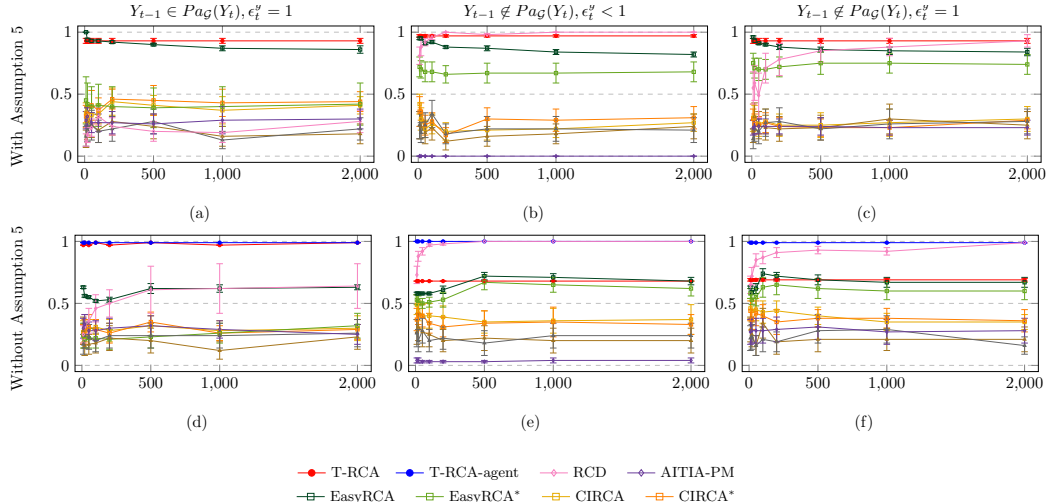


Figure 8: Mean of F1-score averaged over 50 simulations, and associated variance, for other three settings based on T-DSCM, the lengths of \mathcal{D}_{on} varying from 10 to 2,000.

the performance of T-RCA decreases significantly compared to the former one. In both cases, CIRCA demonstrates similar performance to CIRCA*. These aforementioned methods clearly outperform AITIA-PM, RCD, EasyRCA*, CloudRanger, and MicroCause.

C.2 Extension of Section 5.2.1 - new data generating process

In addition to the setting discussed in Section 5.2.1, we explore three other settings based on T-DSCM, varying the lengths of the online set, \mathcal{D}_{on} , from 10 to 2,000 samples. Firstly, we distinguish if self-causes are considered for each vertex in the T-SCG or not (denoted as $Y_{t-1} \in Pa_{\mathcal{G}}(Y_t)$ or $Y_{t-1} \notin Pa_{\mathcal{G}}(Y_t)$). Secondly, we distinguish $\epsilon_t^y = 1$ (i.e., certainty in anomaly propagation, referred to as $\epsilon_t^y = 1$) and $\epsilon_t^y < 1$ (i.e., uncertainty in anomaly propagation, referred to as $\epsilon_t^y = 1 - 0.3^{|Pa_{\mathcal{G}_{\text{fl}}}(Y_t) \cap \mathbb{A}|}$).

For the setting, which incorporates self-causes and assumes certainty in anomaly propagation, a variable exhibits an anomalous value at time t if one of its parents in the T-SCG or the variable itself had an anomalous value at $t - 1$. In contrast, in the absence of self-causes, the determination of the anomalous value for a variable does not consider its values at preceding timestamps. In the uncertain propagation scenario, the probability of an anomalous value is

proportional to the number of its anomalous parents; that is, a variable is more likely to have an anomalous value if it has more parents with anomalous values in the graph. We set the probability that the anomaly fails to propagate from one of its parents to the variable itself to 0.3. Similar to previous configurations, for each setting, we consider two cases by distinguishing whether Assumption 5 holds or not.

Results depicting the means and variances of the F1-score for each method are presented in Figure 8. When Assumption 5 holds, T-RCA consistently performs well and ranks high in performance.

However, when Assumption 5 is violated, the performance of T-RCA significantly declines in most scenarios due to the violation of its assumption. Conversely, T-RCA-agent exhibits superior performance with an F1-score close to 1 on average over. Moreover, in settings where anomaly propagation is certain and includes self-causes, T-RCA performs nearly identically to T-RCA-agent. This is attributed to the T-SCG generated by our chosen causal discovery method containing several strongly connected components (SCC). By utilizing temporal information in \mathcal{D}_{on} , T-RCA can effectively identify the root cause(s) in this specific case.

EasyRCA performs better when Assumption 5 holds compared to when it is violated. In most cases, the performance of RCD tends to improve with the expansion of the length of \mathcal{D}_{on} , especially excelling in settings without self-causes, occasionally achieving optimal performance. However, when self-causes are present, the performance of RCD tends to decline. This is because RCA utilizes PC to uncover variable relationships without considering temporal relations. Additionally, it is worth noting that RCD discretizes time series, which aids in root cause detection within settings based on T-DSCM. Similarly, EasyRCA* also performs better in cases without self-causes, while EasyRCA consistently outperforms EasyRCA*. CIRCA and CIRCA* have comparable performance across all cases.

C.3 Robustness according to the choice of the threshold - equal thresholds

In this section, we test the robustness of T-RCA by checking its performance when we choose the same threshold for all time series, a scenario which is unlikely to occur in practice. We examine this performance across various threshold values

C.3.1 Simulated data

For our proposed methods, T-RCA and T-RCA-agent, thresholds are required for binarizing each time series. Here, we aim to investigate how changes in thresholds impact the performance of our proposed methods across the same cases outlined in Section 5.2. We vary the threshold for each variable by controlling the proportion of data below this threshold in \mathcal{D}_{off} from 0.8 to 0.98 in steps of 0.02. Specifically, a proportion of 0.8 implies that the threshold for each time series is chosen to ensure that 80% of data in \mathcal{D}_{off} are smaller than this threshold.

In the setting of T-DSCM, results depicting the means and variances of the F1-scores are presented in Figure 9 (a and d), where the dashed line illustrates the performance of the method when the thresholds are correctly chosen for each time series. However, for the other two settings, true thresholds for the time series do not exist, hence there are no dashed lines in the corresponding results. The solid line illustrates the performance of the method with varying thresholds, which does not surpass the dashed line for each method. This is because, during the data generating process, the threshold is randomly chosen for each time series, potentially resulting in different thresholds in practice. However, for simplicity, we adopt the same rule to choose the threshold for each time series, which does not guarantee that the threshold for each variable is properly chosen. It is worth noting that in the setting based on T-DSCM, correctly chosen thresholds aid our proposed method in detecting root causes. As the relationship between two variables in this setting depends on thresholds, choosing thresholds higher than the correct one reduces examples for the relations where anomaly causes anomaly, thereby decreasing the performance of our method. Similarly, choosing thresholds lower than the correct one includes examples that do not accurately represent the relations where anomaly causes anomaly, also reducing the performance of our method. Overall, in this setting, the performance of our proposed methods fluctuates with changes in thresholds, but generally, the variance remains within an acceptable range. Practically, the threshold value associated with the highest performance of our proposed methods can serve as a reference for selecting the optimal threshold to monitor the time series.

For settings corresponding to Section 5.2.2 and Section 5.2.3, results depicting the means and variances of the F1-scores are presented in Figure 9 (b and e) and Figure 9 (c and f), respectively. In these settings, the performance of our proposed methods remains consistent with low variance when varying the thresholds, as the causal mechanisms in these two settings are continuous.

From the results above, we can conclude that if the causal mechanism is based on thresholds, such as event-based relations, misspecification of the threshold for time series will degrade the performance of our proposed method. However,

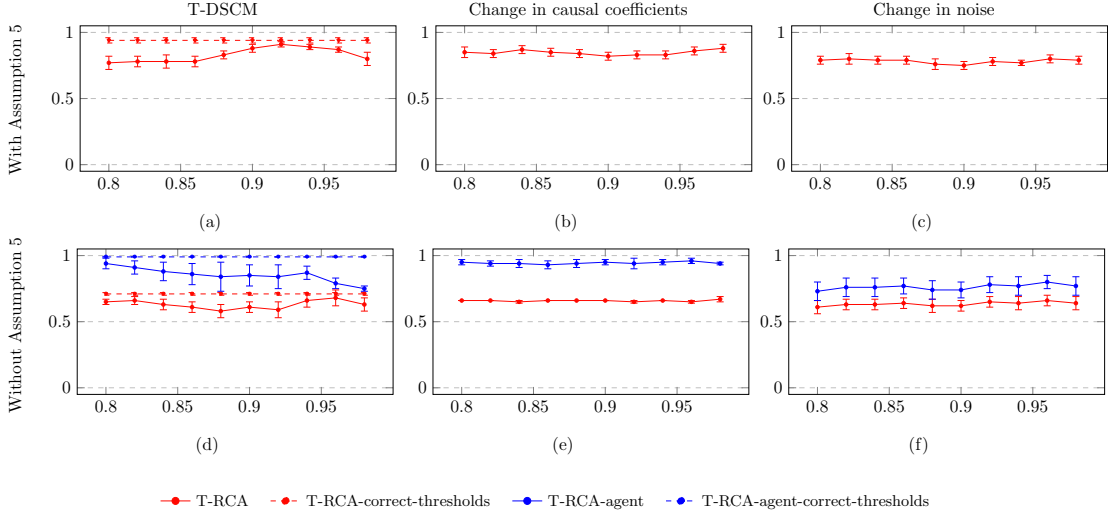


Figure 9: Mean of the F1-score, averaged over 50 simulations, and associated variance, for the three data generating processes of our proposed methods. We vary the threshold for each time series by controlling the proportion of data smaller than this threshold in \mathcal{D}_{off} from 0.8 to 0.98 in steps of 0.02. The dashed line represents the performance of the methods when the thresholds of time series are correctly chosen

when the causal mechanism is continuous, misspecification of the threshold for time series will not significantly impact the performance of our proposed method.

C.3.2 Real IT monitoring data

Similarly, we vary the threshold for each time series by controlling the proportion of data smaller than this threshold in \mathcal{D}_{off} from 0.8 to 0.98 in steps of 0.02 on real IT monitoring data, and the F1-score is shown in Figure 10. When thresholds are chosen much lower than the correct one, examples that inaccurately represent the relations where anomaly causes anomaly are included, leading to a decline in the performance of T-RCA. Then, with the increasing of thresholds, the performance of T-RCA tends to increase. Except, at the point where the proportion is 0.94, the performance of the method exhibits significant variance compared to nearby points, as we adopt the same rule to choose the threshold for each time series for simplicity. However, in practice, the correct threshold for each time series may vary.

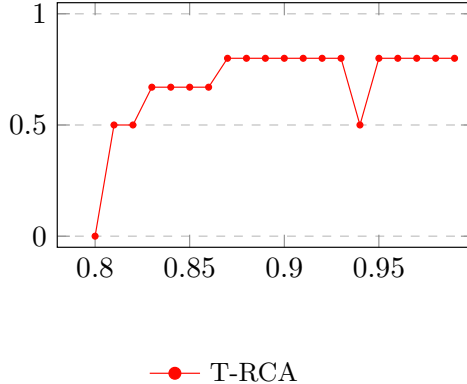


Figure 10: F1-score on Real IT monitoring data for our method, varying the threshold for each time series by controlling the proportion of data smaller than this threshold in \mathcal{D}_{off} from 0.8 to 0.98 in steps of 0.02.

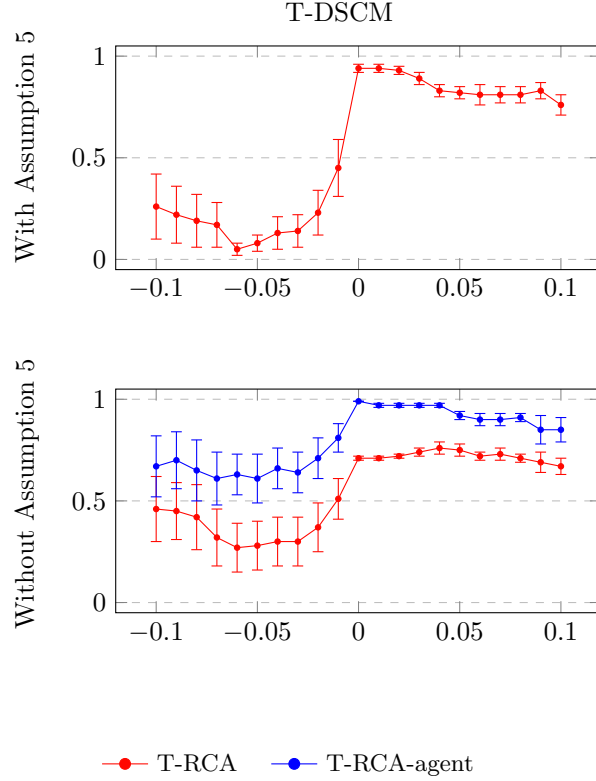


Figure 11: Mean of the F1-score, averaged over 50 simulations, and associated variance, for the data generating processes based on T-DSCM of our proposed methods. We varied the thresholds for each time series by offsetting them from the correct thresholds, ranging from -1 to 1 in steps of 0.01.

C.4 Robustness according to the choice of the threshold - different thresholds

C.4.1 Simulated data

We also tested how good our method is when the threshold is incorrect. In other words, we also tested the performance of our method when the threshold is not correctly specified. To do this, we vary the thresholds for each time series by offsetting them from the correct thresholds, ranging from -1 to 1 in steps of 0.01.

The results given in Figure 11 which shows that when the specified threshold is a higher than the true threshold then T-RCA (and T-RCA-agent) manage to keep a good performance. This means that when a system expert is hesitating between two different values (but not significantly different) for the threshold, it is better to choose the higher one.

C.4.2 Real IT monitoring data

Since we do not have the true thresholds for each time series, we start here by fine-tuning the thresholds that gives the best results then we perform then same analysis that was done for simulated data.

Fine-tuning thresholds To fine-tune the thresholds we tested randomly several threshold and selected the one that gives the highest F1-score.

Surprisingly, we were able to find several sets of thresholds for which T-RCA can identify the root causes with an F1-score equals to 1. This might confirms, that our system is threshold-based.

Varying thresholds with respect to the fine-tuned thresholds

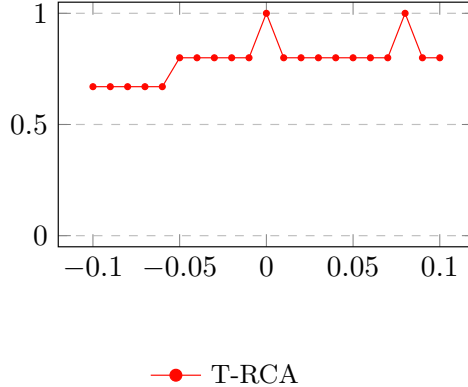


Figure 12: F1-score on Real IT monitoring data for our method, varying the threshold for each time series by offsetting them from the fine-tuning thresholds. We varied the thresholds from -1 to 1 in steps of 0.01. Specifically, for RTMB, due to its small values, we adjusted its threshold from -0.001 to 0.001 in steps of 0.0001.

Here we choose the thresholds that correspond to the smallest values for which T-RCA can identify the root causes with an F1-score equals to 1.

As before, we vary the thresholds for all time series by iteratively decreasing the fine-tuned thresholds by 0.01 or increasing them by 0.01, repeated five times on each side. However, an exception is made for the time series RTMB, where we decrease and increase the thresholds by 0.0001. This exception is warranted as all values of this time series are smaller than 0.01.

The results given in Figure 12, again which again shows that if a system expert is undecided between two slightly different threshold values, it is better to opt for the higher one.